TEP/EDTA Doubly Regulated Hydrothermal Crystallization of Hydroxyapatite Films on Metal Substrates

Daniel J. Haders,[†,‡] Alexander Burukhin,[†] Eugene Zlotnikov,[†] and Richard E. Riman*[,†,‡]

Department of Material Science and Engineering, Rutgers, The State University of New Jersey, 607 Taylor Road, Piscataway, New Jersey 08854, and Department of Biomedical Engineering, Rutgers, The State University of New Jersey, 599 Taylor Road, Piscataway, New Jersey 08854

Received June 18, 2007. Revised Manuscript Received June 30, 2008

The aim of this study was to investigate the use of $Ca(EDTA)^{2-}$ and triethyl phosphate (TEP) to regulate the hydrothermal crystallization of hydroxyapatite (HA) films. HA was coated on various substrates including titanium, Ti6Al4V, grit-blasted Ti6Al4V, 316 stainless steel, and Co28Cr6Mo via hydrothermal synthesis at 200 °C for 24 h utilizing a 0.232 molal $Ca(NO_3)_2$−0.232 molal EDTA−0.187 molal TEP−1.852 molal KOH−H_2O chemical system. The role of film deposition processing variables on HA crystallization was studied using thermodynamic process simulation and experimental TEP hydrolysis kinetics data. Profilometry, XRD, FESEM, and adhesion testing (ASTM D3359) were used to characterize substrates and films. Kinetics studies of TEP hydrolysis revealed that phosphate was available for the formation of HA at temperatures above 180 °C and synthesis times greater than 4 h. Thermodynamic modeling demonstrated both that the formation of phase pure HA was thermodynamically favored at 200 °C on all substrates and that the equilibrium concentration of free Ca^{2+} was lower in this system than in hydrothermal HA film crystallization systems reported elsewhere. Materials characterization results indicate that high crystallinity (99+%), (0002) crystallographically oriented, passivating, Ca−P (calcium-phosphate) phase pure HA films composed of hexagonal faceted grains (8−12 μm diameter) were formed on all substrates. On the basis of these results, it is concluded that the use of TEP necessitates a continuous two-step film deposition process that deposits phase pure HA at temperatures above 180 °C. The use of $Ca(EDTA)^{2-}$/pH regulation of Ca^{2+} concentration enables the hydrothermal HA crystallization process to be growth dominated, producing films composed of high crystallinity, hexagonal grains.

The ceramic phase of bone is a poorly crystalline, anion/cation-substituted, nonstoichiometric hydroxyapatite (HA), $Ca_{10}(PO_4)_6(OH)_2$.[1−3] Because of its biocompatibility, HA is considered the preferred material for hard tissue replacement.[3,4] However, the poor mechanical properties and low reliability of HA necessitates the use of bioinert metals, which often become encapsulated by fibrous tissue in vivo, in load-bearing orthopedic applications.[3−7] Consequently, attention has been given to HA coatings for metallic orthopedic implants in an effort to take advantage of the bioactivity of HA and the mechanical properties of clinically used metals.[3,4] Numerous reviews have described how HA-coated metallic orthopedic implants bridge larger gaps between the implant and bone with new bone tissue, accelerate bone apposition, are more tolerant of osteoporotic bone, and have increased bone-implant bond strength as compared with alternative orthopedic implant surfaces including sintered metallic coatings, plasma-sprayed titanium coatings, and roughened or untreated metallic implant surfaces.[3,6,8−13]

Commercially, most hydroxyapatite coatings are applied using plasma spray methods (PS-HA).[3,10,12−15] Conceptually simple, the process has many variables, which result in coatings of inconsistent quality with variable crystallinity and variable percentages of secondary and amorphous phases.[3,13−18] Since the introduction of PS-HA coatings in the 1980s,[3] numerous studies have raised concern about the consequences of PS-HA's high resorption

* Corresponding author. Tel.: (732) 445-4946. Fax: (732) 445-6264. E-mail: riman@rci.rutgers.edu.
† Department of Material Science and Engineering, Rutgers, The State University of New Jersey.
‡ Department of Biomedical Engineering, Rutgers, The State University of New Jersey.

(1) Boskey, A. L.; Posner, A. S. *Orthop. Clin. North Am.* **1984**, *15*, 597–612.
(2) Daculsi, G.; Bouler, J. M.; LeGeros, R. Z. *Int. Rev. Cytol.* **1997**, *172*, 129–191.
(3) Sun, L.; Berndt, C. C.; Gross, K. A.; Kucuk, A. *J. Biomed. Mater. Res.* **2001**, *58*, 570–592.
(4) Suchanek, W.; Yoshimura, M. *J. Mater. Res.* **1998**, *13*, 94–117.
(5) Porter, A. E.; Taak, P.; Hobbs, L. W.; Coathup, M. J.; Blunn, G. W.; Spector, M. *Biomaterials* **2004**, *25*, 5199–5208.
(6) Dunn, M. G.; Maxian, S. H. *J. Long-Term Eff. Med. Implants* **1991**, *1*, 193–203.
(7) Spivak, J. M.; Ricci, J. L.; Blumenthal, N. C.; Alexander, H. *J. Biomed. Mater. Res.* **1990**, *24*, 1121–1149.
(8) Bauer, T. W.; Schils, J. *Skeletal Radiol.* **1999**, *28*, 423–432.
(9) Capello, W. N.; D'Antonio, J. A.; Manley, M. T.; Feinberg, J. R. *Clin. Orthop. Relat. Res.* **1998**, 200–211.
(10) Thomas, K. A. *Orthopedics* **1994**, *17*, 267–278.
(11) LeGeros, R. Z.; Craig, R. G. *J. Bone Miner. Res.* **1993**, *8 Suppl 2*, S583−596.
(12) Dumbleton, J.; Manley, M. T. *J. Bone Joint Surg. Am.* **2004**, *86-A*, 2526–2540.
(13) Geesink, R. G. *Clin Orthop Relat Res* **2002**, 53–65.
(14) Cheang, P.; Khor, K. A. *Biomaterials* **1996**, *17*, 537–544.
(15) Tsui, Y. C.; Doyle, C.; Clyne, T. W. *Biomaterials* **1998**, *19*, 2015–2029.
(16) Dalton, J. E.; Cook, S. D. *J. Biomed. Mater. Res.* **1995**, *29*, 239–245.
(17) Park, E.; Condrate, R. A.; Hoelzer, D. T.; Fischman, G. S. *J. Mater. Sci. Mater. Med.* **1998**, *9*, 643–649.
(18) Ji, H.; Ponton, C. B.; Marquis, P. M. *J Mater. Sci. Mater. Med.* **1992**, *3*, 283–287.

10.1021/cm071628c CCC: $40.75
Published on Web 10/24/2008

rates,[3,5,16,19] which are reported to reduce bone apposition; poor adhesion properties,[3,15,17,18,20] which have resulted in coating delamination in vivo;[3,7,11,21,22] inability to passivate metal substrates,[23] which permits the release of toxic metal ions into the body;[24,25] and line-of-sight limitations, which result in an inability to coat the internal surfaces of porous or curved three-dimensional structures.[13] Therefore, there is a need to develop inexpensive reproducible crystallization processes, which deposit high crystallinity, phase pure, nonresorbing, adhesive, passivating, conformal HA films on metallic substrates.

The literature reports numerous additional HA film synthesis techniques including sol−gel, pulsed laser deposition, magnetron sputtering, ion-beam deposition, biomimetic, and hydrothermal crystallization.[4] Sol−gel, magnetron sputtering, pulsed laser deposition, and ion-beam deposition require postdeposition high-temperature heat-treatment to increase crystallinity, density, and often phase purity, and the latter three are line-of-sight limited processes.[26−29] Biomimetic deposition requires multiday syntheses to produce low crystallinity films.[30] However, non-line-of-sight, solution-mediated hydrothermal crystallization has many of the qualities necessary to obtain the films outlined in the previous paragraph. Numerous authors have shown that by regulating processing variables, it is possible to dictate the direct crystallization of desired phases from homogeneous solutions using this technique.[31,32] Specifically, a number of authors have reported hydrothermal crystallization processes that synthesize phase pure, crystalline, HA films.[33−38] Substrates including titanium, alumina, calcium titanate, monetite, doped tetragonal zirconia, iron, aluminum, and copper have been coated with HA using these methods.[33−39]

The literature, however, highlights drawbacks of current HA hydrothermal processes. Authors using multiple substrates have reported substrate-dependent and roughness-dependent effects on precipitation behavior, and films formed on titanium, calcium titanate, aluminum, copper, doped tetragonal zirconia, and alumina are a combination of nonuniform, low-density, and nonpassivating.[33,36−39] In one study, cross-sections of films formed on alumina are uniform and appear dense and passivating; however, these claims are not specifically made and the authors do not report additional studies on multiple substrates.[40] Hexagonal grains of HA are known to display the $\{10\bar{1}0\}$ crystallographic plain, which has been shown to bind bone proteins and bone protein amino acid sequences with high affinity.[41−43] Grain morphology on iron, aluminum, copper, titanium, calcium titanate, doped tetragonal zirconia, and alumina substrates is limited to plate-, needle-, or rodlike, with diameters less than 5 μm and often near 1 μm, however.[36−39] Two-step processes that use one reaction solution to deposit $CaTiO_3$ and another to deposit HA are required to form both an interfacial layer, which improves film−substrate adhesion, and HA on the clinically relevant Ti6Al4V alloy (alloyed titanium with 6 wt % aluminum and 4 wt % vanadium).[33,37,39] Therefore, there is a need to develop hydrothermal HA crystallization processes that deposit uniform, dense, passivating, hexagonal grained HA films on multiple substrates, in addition to a $CaTiO_3$ interfacial layer on titanium substrates, in a single continuous process.

Limitations in the current hydrothermal HA crystallization literature may be overcome by doubly regulating the concentration of Ca^{2+} and PO_4^{3-} ions in the homogeneous reaction solution. Ethylenediamine-tetraacetic acid ($EDTA^{4-}$) is often used to chelate calcium ions to regulate the concentration of uncomplexed Ca^{2+} and control HA nucleation and growth on substrates.[34−39] It has been reported, however, that temperature and pH affect the dissociation of the $Ca(EDTA)^{2-}$ complex.[34,36,38] Therefore, by controlling temperature and pH, uncomplexed Ca^{2+} concentration may be further regulated, enabling the engineering of growth-dominated film crystallization processes that result in films that have a characteristic shape, hexagonal for HA, and high crystallinity.[44] Results from the literature have also demonstrate that HA grain aspect ratio may be controlled by regulating Ca^{2+} concentration together with EDTA/Ca ratio, temperature, and pH.[45,46] There are no reports of HA hydrothermal methods that control film nucleation and growth by regulating the concentration of free PO_4^{3-}. One

(19) Klein, C. P.; Wolke, J. G.; de Blieck-Hogervorst, J. M.; de Groot, K. *J. Biomed. Mater. Res.* **1994**, *28*, 909–917.
(20) Filiaggi, M. J.; Coombs, N. A.; Pilliar, R. M. *J. Biomed. Mater. Res.* **1991**, *25*, 1211–1229.
(21) Kangasniemi, I. M.; Verheyen, C. C.; van der Velde, E. A.; de Groot, K. *J. Biomed. Mater. Res.* **1994**, *28*, 563–572.
(22) Lin, H.; Xu, H.; Zhang, X.; de Groot, K. *J. Biomed. Mater. Res.* **1998**, *43*, 113–122.
(23) Browne, M.; Gregson, P. J. *Biomaterials* **2000**, *21*, 385–392.
(24) Okazaki, Y.; Gotoh, E.; Manabe, T.; Kobayashi, K. *Biomaterials* **2004**, *25*, 5913–5920.
(25) Puleo, D. A.; Huh, W. W. *J. Appl. Biomater.* **1995**, *6*, 109–116.
(26) Wang, D.; Chen, C.; Liu, X.; Lei, T. *Colloids Surf., B* **2007**, *57*, 237–242.
(27) van Dijk, K.; Schaeken, H. G.; Wolke, J. G.; Jansen, J. A. *Biomaterials* **1996**, *17*, 405–410.
(28) Ong, J. L.; Lucas, L. C. *Biomaterials* **1994**, *15*, 337–341.
(29) Garcia, F.; Arias, J. L.; Mayor, B.; Pou, J.; Rehman, I.; Knowles, J.; Best, S.; Leon, B.; Perez-Amor, M.; Bonfield, W. *J. Biomed. Mater. Res.* **1998**, *43*, 69–76.
(30) Jonasova, L.; Muller, F. A.; Helebrant, A.; Strnad, J.; Greil, P. *Biomaterials* **2004**, *25*, 1187–1194.
(31) Byrappa, K.; Yoshimura, M. *Handbook of Hydrothermal Cystallization*; Noyes Publications: Park Ridge, NJ, 2001.
(32) Riman, R. E.; Suchanek, W. L.; Lencka, M. M. *Ann. Chim. (Sci. Mater.)* **2002**, *27*, 15–36.
(33) Ohba, Y.; Watanabe, T.; Sakai, E.; Daimon, M. *J. Ceram. Soc. Jpn.* **1999**, *107*, 907–912.
(34) Toriyama, M.; Kawamoto, Y.; Suzuki, T.; Yokogawa, Y.; Nishizawa, K.; Nagata, F.; Mucalo, M. R. *J. Mater. Sci. Lett.* **1996**, *15*, 179–181.
(35) Jung-Soo Ha. Rahaman, M. N. *Ceram. Eng. Sci. Proc.* **2003**, *24*, 239–244.
(36) Fujishiro, Y.; Sato, T.; Okuwaki, A. *J. Mater. Sci.: Mater. Med.* **1995**, *6*, 172–176.
(37) Fujishiro, Y.; Sugimori, A.; Okuwaki, A.; Sato, T. *J. Mater. Sci. Mater. Med.* **2001**, *12*, 333–337.
(38) Fujishiro, Y.; Fujimoto, A.; Sato, T.; Okuwaki, A. *J. Colloid Interface Sci.* **1995**, *173*, 119–127.
(39) Fujishiro, Y.; Sato, N.; Uchida, S.; Sato, T. *J. Mater. Sci. Mater. Med.* **1998**, *9*, 363–367.
(40) Ha, J. S.; Rahaman, M. N. *Ceram. Eng. Sci. Proc.* **2003**, *24*, 239–244.
(41) Kirkham, J.; Brookes, S. J.; Shore, R. C.; Wood, S. R.; Smith, D. A.; Zhang, J.; Chen, H.; Robinson, C. *Curr. Opin. Colloid Interface Sci.* **2002**, *7*, 124–132.
(42) Huq, N. L.; Cross, K. J.; Reynolds, E. C. *J Mol. Model.* **2000**, *6*, 35–47.
(43) Fujisawa, R.; Kuboki, Y. *Biochim. Biophys. Acta* **1991**, *1075*, 56–60.
(44) Klein, C.; Hurlbut, C.; Dana, J. D. *Manual of Mineralogy*, 20th ed.; John Wiley & Sons: New York, 1985,

potential route would be to use triethyl phosphate (TEP), which requires completion of a three-step hydrolysis reaction to release PO_4^{3-} ions

$$(C_2H_5O)_3PO + H_2O \rightarrow [(C_2H_5O)_2P(O)_2]^- + C_2H_5OH + H^+ \quad (1)$$

$$[(C_2H_5O)_2P(O)_2]^- + H_2O \rightarrow [(C_2H_5O)P(O)_3]^{2-} + C_2H_5OH + H^+ \quad (2)$$

$$[(C_2H_5O)P(O)_3]^{2-} + H_2O \rightarrow PO_4^{3-} + C_2H_5OH + H^+ \quad (3)$$

Research describing the hydrolysis of TEP and related trialkyl phosphates has been reported in the literature.[47−49] At or below 110 °C the first ethoxide group hydrolyzes rapidly in a base- or neutral-catalyzed reaction relative to the second and third ethoxide groups, which hydrolyze in an acid-catalyzed reaction.[47,48] Kinetics studies of the hydrolysis of the first group at 110 °C show that the reaction rate increases with pH.[47] Base-catalyzed hydrolysis of dimethyl phosphate (DMP) is reported in strong alkali solutions at higher temperatures (115−125 °C).[49] By delaying the release of uncomplexed phosphate ions, reactions involving calcium ions and the substrate may be initiated to form substrate−HA intermediate layers. One possibility would be reacting Ca^{2+} with titanium substrates to form $CaTiO_3$. Therefore, through control of temperature and pH and use of TEP and EDTA reagents there exists the potential to doubly regulate the concentration of uncomplexed Ca^{2+} and PO_4^{3-} ions, and consequently, the size, morphology, crystallinity, and adhesion of HA films.

To intelligently engineer the crystallization process, we may utilize thermodynamic calculations and models to identify the equilibrium phase space (i.e., temperature, pH, reagent concentration combinations) required to produce HA from fundamental principles.[32,38,50] This approach reduces or eliminates time-consuming trial and error laboratory methods.[32,50] Riman et al. has previously validated the process of defining HA processing variable space using thermodynamic software, and then synthesizing HA particles based on those diagrams.[50]

This study reports the first use of EDTA/TEP doubly regulated hydrothermal crystallization of hydroxyapatite films on multiple substrates. The study explores the kinetics of TEP hydrolysis and the thermodynamics of free calcium concentration and HA phase equilibria, as well as the effect of substrate on the microstructure, thickness, constituent phases, crystallinity, and adhesion of HA films.

Experimental Section

(a) Thermodynamic Process Simulation. Thermodynamic phase equilibria models were calculated using thermo-chemical simulation software (OLI Systems, Inc., Morris Plains, NJ). The fundamental basis for the algorithms used in the software is reported in Lencka and Riman.[51] HA thermodynamic phase equilibria models for the $CaO-P_2O_5-NH_4NO_3-H_2O$ chemical system are reported in Riman et al.[50]

Experimental conditions for hydrothermal crystallization of HA films in the $Ca(NO_3)_2$−EDTA−TEP−KOH−H_2O chemical system were chosen based upon calculated phase boundaries of the $Ca(NO_3)_2$−EDTA−H_3PO_4−KOH−H_2O system in the presence of titanium, 316 stainless steel (Fe−Cr−Ni), and Co−Cr at 200 °C. These metals were considered representative of the substrates used in this work (Ti6Al4V, grit blasted Ti6Al4V, Ti, 316 stainless steel, Co28Cr6Mo, see below), which were chosen on the basis of their current or prior use in clinical load bearing orthopedic applications. The software database does not contain TEP because there is no reported thermodynamic data for TEP in the literature. Thus, H_3PO_4 was utilized in its place for thermodynamic calculations. The use of this acid allows the model to account for products of TEP hydrolysis, PO_4^{3-} and $3H^+$, without the explicit use of TEP. This substitution was justified by reviewing the phosphate chemical species calculated to be present at 200 °C in the 0.232 molal $Ca(NO_3)$−0.232 molal EDTA−0.187 molal H_3PO−1.852 molal KOH−Ti−H_2O chemical system. The data demonstrated that H_3PO_4 is calculated to have a concentration of less than 1×10^{-10} molal at 200 °C, which indicates that H_3PO_4 "releases" free phosphate and is a reasonable model for TEP at 200 °C. TEP kinetics results, reported below, indicate that complete hydrolysis occurs at 180 °C, which validates the substitution of H_3PO_4 for TEP in the model at 200 °C. The third product of TEP hydrolysis, C_2H_5OH, was ignored because of its dilute state in the solution, 0.561 molal, after full TEP hydrolysis. This omission was justified by comparing the phase diagrams of the 0.232 molal $Ca(NO_3)$−0.232 molal EDTA−0.187 molal H_3PO_4−1.852 molal KOH−Ti−H_2O chemical system and the 0.232 molal $Ca(NO_3)$−0.232 molal EDTA−0.187 molal H_3PO_4−0.561 molal C_2H_5OH−1.852 molal KOH−Ti−H_2O chemical system at 200 °C. A comparison of the two diagrams demonstrated no differences in the position of phase boundaries at pH relevant to the work in this study. After the creation of phase diagrams, the specific pH/Ca^{2+} combination for the 0.232 molal $Ca(NO_3)_2$−0.232 molal EDTA−0.187 molal H_3PO_4−1.852 molal KOH−H_2O chemical system used for synthesis in this paper, see below, in the presence of each substrate at 200 °C was calculated and plotted on each respective diagram.

(b) TEP Hydrolysis Kinetics and Reactor Heating Dynamics. To characterize the release of phosphate ions from TEP, we prepared model mixtures containing KOH (Fisher Scientific Hampton, NH) and TEP (Sigma Aldrich, St. Louis, MO). KOH and TEP were dissolved in deionized water at the same concentrations used for synthesis, see below, and loaded into a 1 L stirred Teflon-lined autoclave (Model 4531, Parr Instruments, Moline, IL). The autoclave was equipped with a needle valve with dip tube that allowed sampling at elevated pressure and temperature. Excess calcium nitrate tetrahydrate (Fisher Scientific) was added to samples of reaction products of TEP hydrolysis taken from the reactor at various temperatures to monitor free phosphate formation. The solution was filtered and assayed for the presence of Ca−P precipitate. To evaluate the heating rate of the reaction solution, autoclave heating dynamics were investigated by directly placing K-type thermocouples into 125 mL Parr 4731 autoclaves filled with a model nonvolatile liquid, technical grade glycerol. Autoclaves were placed in an oven preheated to 200 °C, and internal changes in temperature were monitored with time. Heating dynamics were

(45) Andres-Verges, M.; Fernandez-Gonzales, C.; Martinez-Gallego, M. *J. Eur. Ceram. Soc.* **1998**, *18*, 1245–1250.
(46) Fujishiro, Y.; Yabuki, H.; Kawamura, K.; Sato, T.; Okuwaki, A. *J. Chem. Technol. Biotechnol.* **1993**, *57*, 349–353.
(47) Shu, P.; Schmitt, K. *Colloids Surf., A* **1996**, *110*, 273–285.
(48) Barnard, P. W. C.; Bunton, C. A.; Llewellyn, D. R.; Vernon, C. A.; Welch, V. A. *J. Chem. Soc.* **1961**, 2670.
(49) Kumamoto, J.; Cox, J. R.; Westheimer, F. H. *J. Am. Chem. Soc.* **1956**, *78*, 4858–4860.
(50) Riman, R. E.; Suchanek, W. L.; Byrappa, K.; C.W., C.; Shuk, P.; Oakes, C. S. *Solid State Ionics* **2002**, *151*, 393–402.
(51) Lencka, M. M.; Riman, R. E. *Chem. Mater.* **1993**, *5*, 61–70.

compared to TEP hydrolysis kinetics to determine the reaction time above which uncomplexed PO_4^{3-} was available for formation of HA.

(c) Equilibrium Ca^{2+} Concentration. Equilibrium Ca^{2+} concentrations were calculated using commercial thermochemical simulation software referred to previously (OLI Systems, Inc.). The equilibrium concentration of Ca^{2+} was calculated for temperatures from 25−180 °C in the 0.232 molal $Ca(NO_3)_2$−0.232 molal EDTA−1.852 molal KOH−H_2O system in the presence of Ti. This model predicts the concentration of Ca^{2+} prior to complete TEP hydrolysis (see below). Because of the absence of TEP in the software database (see above), the results from the model do not take into account the products of partial TEP hydrolysis, $2H^+$ and $2C_2H_5OH$. The omission of C_2H_5OH is justified in section a (Thermodynamic Process Simulation), above. The omission of $2H^+$ is justified by comparing the pH calculated for the 0.232 molal $Ca(NO_3)_2$−0.232 molal EDTA−1.852 molal KOH−Ti−H_2O system at 180 °C (pH 10.91) and the 0.232 molal $Ca(NO_3)$−0.232 molal EDTA−0.187 molal H_3PO_4−1.852 molal KOH−Ti−H_2O at 180 °C (pH 10.6). A comparison of the pH of each solution demonstrates that the addition ∼0.561 molal of H^+ from the dissociation of H_3PO_4, nominally TEP, at 180 °C minimally changes the pH of the solution. For comparison, the concentration of Ca^{2+} was calculated for temperatures from 25−160 °C (initial HA deposition temperature) in the 0.05 molal $Ca(EDTA)^{2-}$−0.05 molal NaH_2PO_4−NaOH−H_2O−Ti hydrothermal synthesis system, demonstrated by Fujishiro et al. to form phase pure HA.[38] Equilibrium Ca^{2+} concentrations at the initial HA deposition temperature of the system presented here, 180 °C (see below), and the system reported by Fujishiro et al., 160 °C, were compared to evaluate the thermodynamic effect of pH and temperature on uncomplexed Ca^{2+} concentration and to predict/explain morphological differences between the two films.

(d) Film Synthesis. Metal substrates (Ti6Al4V, grit blasted Ti6Al4V, Ti, 316 stainless steel, Co28Cr6Mo) were chosen based on their current or prior use in clinical load bearing orthopedic applications. The choice of substrates enabled an investigation of the ability of the crystallization process to uniformly coat substrates with various chemistries and surface roughnesses with HA. The choice of substrates also enabled an investigation of the effect of crystallography on HA deposition; Ti6Al4V, grit blasted Ti6Al4V, Ti, and Co28Cr6Mo have hexagonal crystal lattices and 316 stainless steel has a cubic lattice.

Prior to synthesis, 1 in diameter rods of Ti6Al4V alloy (ASTM-B348 grade 5, McMaster Carr, Dayton, NJ), titanium (98.9% pure, ASTM-B348 grade 2, McMaster Carr), 316 stainless steel (ASTM-A276, McMaster Carr), and Co28Cr6Mo alloy (ASTM-F75, Stryker Orthopaedics, Mahwah, NJ) were cut into discs, 1 in. (diameter) × 1/8 in. (thickness), and used as substrates. Where indicated, Ti6Al4V alloy substrates were grit-blasted using 35−100 Al_2O_3 media (McMaster Carr) to roughen the surface. Grit was removed by cleaning in an ultrasonic bath (FS30, Fisher Scientific). All substrates, titanium foil (0.127 mm, 99.7%, Sigma-Aldrich) substrate holders, and Teflon reaction vessel liners (125 mL, Parr Instrument) were cleaned with Citronox detergent (Alconox, White Plains, NY), acetone (Fisher Scientific), ethyl alcohol (Pharmco-AAPER, Brookfield, CT), and deionized water and dried in a 60 °C oven prior to synthesis.

Aqueous stock solutions of 0.232 molal calcium nitrate tetrahydrate, $Ca(NO_3)_2 \cdot 4H_2O$ (99.38%, Fisher Scientific), 0.232 molal ethylenediamine-tetraacetic acid (EDTA), $C_{10}H_{16}N_2O_8$ (99.4%, Fisher Scientific), 0.187 molal triethyl phosphate (TEP), $C_6H_{15}O_4P$ (99.8+ %, Sigma Aldrich), and 1.852 molal potassium hydroxide, KOH (89.3%, Fisher Scientific) were used for hydrothermal reactions and prepared as follows:

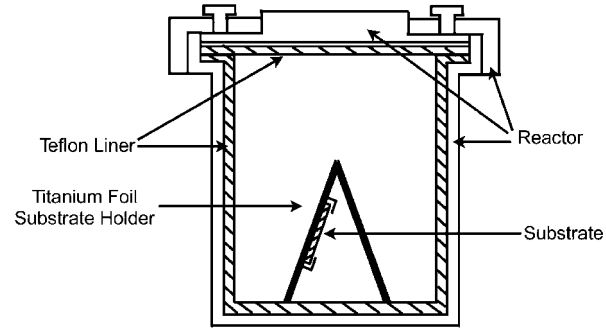

Figure 1. Cross-sectional diagram of a Parr (model 4731) reactor.

Calcium nitrate tetrahydrate, EDTA, and TEP were mixed together and dissolved in deionized H_2O. In a second container, KOH was dissolved in deionized H_2O. Once dissolved, the KOH solution was placed in a cold-water bath to cool to room temperature. When cool, the KOH solution was added to the former solution and stirred until visible particulates had dissolved. The stock solution was then filtered (220 nm pore size, Nalgene, Rochester, NY) and stored in a tightly sealed container.

The typical hydrothermal reaction was conducted as follows: The substrate was fixed in the substrate holder and placed inside a 125 mL Teflon-lined reaction vessel (4731 reactor, Parr Instrument). The substrate holder placed the sample in a position that inhibited the settling of homogeneously formed nuclei onto the surface by means of gravity (Figure 1). Stock solution, 70 mL, was added to the reaction vessel, which was then sealed. The reactor was then placed in an oven preheated to 200 °C for 24 h. The reactor was removed from the oven and allowed to cool to room temperature in air. The substrate was removed from the reactor and rinsed for several minutes in running tap water and then in deionized water. The sample was then placed in a 60 °C oven to dry.

(e) Substrate and Film Characterization. A profilometer (scan length 500 μm, Dektak 3030, Veeco, Woodbury, NY) was used to measure the surface roughness, Ra, of each substrate. Field emission scanning electron microscopy (FESEM) (DSM 982 Gemini, Carl Zeiss, Oberkochen, Germany) was used to examine the bare substrate and film microstructure in cross-section, top-on, and after adhesion experiments. Cross sectional samples were prepared by cutting two cross-sections from each substrate−film sample with a diamond saw (Vari/Cut VC-50, Leco Corporation, St. Joseph, MI). These were then embedded face-to-face in epoxy (SPI-PON Epoxy Embedding Kit, SPI Supplies, West Chester, PA), polished until substrates achieved a mirror finish, and sputter coated with a conducting 25nm Au/Pd film (Balzers SCD 004, OC Oerlikon Balzers AG, Balzers, Liechtenstein). Film thickness was computed by direct measurement of the thickness of FESEM cross-sections at 22 μm intervals (10 points) along the length of the micrograph using commercial image analysis software. Grain diameter was determined by direct measurement of 10 randomly selected grains shown in top-on FESEM micrographs using commercial image analysis software. Average film thickness, average grain diameter, and the standard deviation of the means were calculated using Excel (Microsoft, Redmond, WA). A two-tailed, heteroscedastic *t* test was used to determine if differences in grain diameters were significant ($\alpha = 0.5$, Microsoft Excel). An estimate of grain aspect ratio was calculated by dividing average film thickness by average grain diameter. The calculation assumes that grains run continuously from the substrate surface to the film surface. X-ray diffraction (XRD) (step size = 0.005 °, 1 step/s, 45 KV, 40 mA, Ni-filtered Cu Kα radiation, parallel beam optics, Philips Hi-Resolution X'PERT

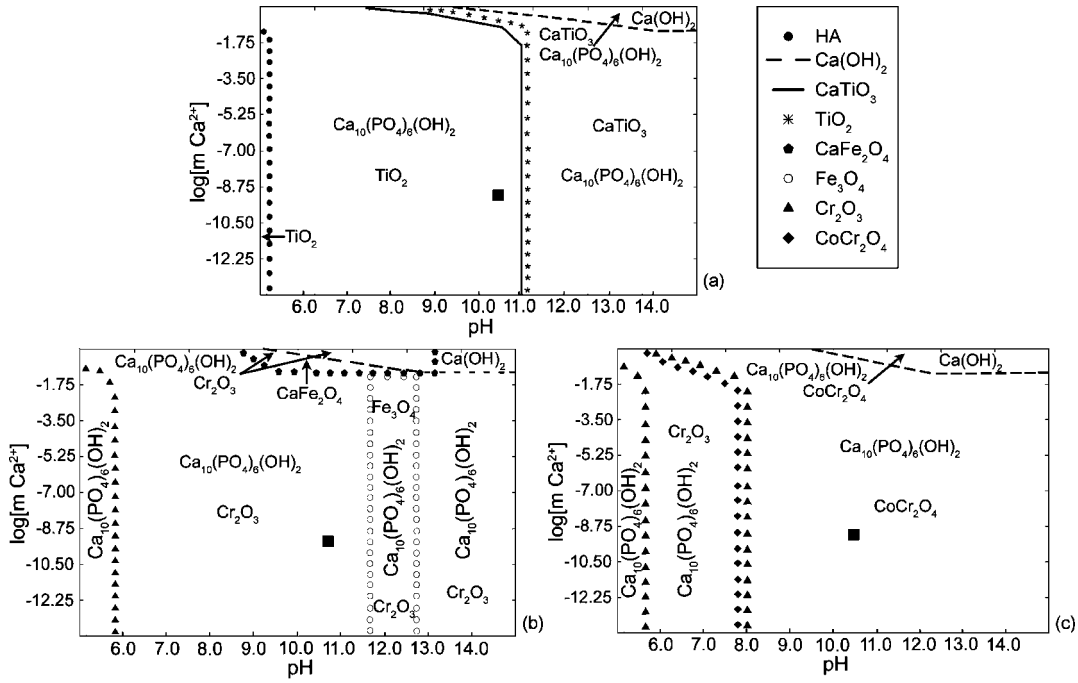

Figure 2. Calculated thermochemical phase equilibria diagram for the 0.232 molal $Ca(NO_3)_2$−0.232 molal EDTA−0.187 molal H_3PO_4−1.852 molal KOH−H_2O chemical system at 200 °C in the presence of various substrates: (a) titanium, (b) 316 stainless steel, (c) Co−Cr. The black box represents the equilibrium pH/[m Ca^{2+}] (m = molal) combination calculated for each system under these conditions. The initial room temperature pH of the starting slurries has been recalculated to the pH at the experimental temperature. From that point the pH has been titrated to higher and lower values.

X-Ray Diffractometer, PANalytical B.V., Almelo, Netherlands) was used to determine the phases present in the films and the substrate. XRD patterns from Co28Cr6Mo and 316 stainless steel substrates were obtained using an additional graphite diffracted beam monochromator (PANalytical B.V.) to remove background fluorescence. Experimental XRD patterns were matched to patterns in the Powder Diffraction File (PDF, ICDD, Newtown Square, PA) database using Jade 6.5 software (MDI, Livermore, CA). Subsequent to curve fitting (Jade 6.5, MDI), the crystallinity of hydroxyapatite was calculated by comparing the area of HA crystalline peaks in the range 28−35° and of the amorphous calcium-phosphate (ACP) hump centered at approximately 30−31° (2θ) using the following equation:[15]

$$X\% = \left[\frac{\sum_{i=1}^{c} A_c}{(\sum_{i=1}^{c} A_c + \sum_{i=1}^{a} A_a)}\right] * 100\% \qquad (4)$$

where ΣA_c is the sum of the areas under all the HA crystalline peaks and ΣA_a is the sum of the area under the ACP hump. Peak intensities were also used to calculate HA (0002)/(21$\bar{3}$1) peak ratios. Peak deconvolution was used to determine (21$\bar{3}$1) peak intensity due to the overlapping peak profiles of the (21$\bar{3}$1) and (11$\bar{2}$2) peaks in the HA profile (Jade 6.5). The adhesion of the film to the substrate was measured using the ASTM (American Society for Testing and Materials, West Conshohocken, Pennsylvania) standard D3359−02 tape test A. Adhesion was rated on a scale of 0−5 with 5 representing no peeling and 0 representing complete removal, as specified by ASTM. Four measurements were averaged and reported for each film. For comparison purposes, Metalastic DTM Acrylic Modified Enamel (Sherwin Williams, Cleveland, OH) with an ASTM D3359 adhesion rating of 5 and Industrial Shop Primer (Aervoe Industries Incorporated, Gardnerville, NV) with an ASTM D3359 adhesion rating of 3 were used as standards.

Results

(a) Thermodynamic Process Simulation. Computed phase stability diagrams for the $Ca(NO_3)_2$—EDTA−H_3PO_4—KOH−H_2O system in the presence of titanium, 316 stainless steel, and Co−Cr substrates at 200 °C are shown in Figure 2a−c. The diagrams illustrate a wide stability range for HA under these conditions. The diagrams also illustrate that titanium, 316 stainless steel, and Co−Cr substrates are not thermodynamically stable, leading to the formation of oxides. The specific pH/[Ca^{2+}] point for the 0.232 molal $Ca(NO_3)_2$—0.232 molal EDTA—0.187 molal H_3PO_4—1.852 molal KOH−H_2O system in the presence of each respective substrate is marked. For each substrate, the pH/[Ca^{2+}] data point lies in a region where both an oxide and hydroxyapatite are stable. These diagrams demonstrate that the formation of Ca−P (calcium−phosphate) phase-pure HA is thermodynamically favored in the presence of all substrates under these reaction conditions and confirm the stability of HA in alkaline solutions.

(b) TEP Kinetics. TEP hydrolysis kinetics were examined under alkaline hydrothermal conditions. Results revealed that Ca−P particles precipitated in samples taken from solutions with temperatures above 180 °C, after the addition of excess calcium nitrate. This agrees with hydrolysis results from the literature, which suggest that temperatures above 110 °C are needed to hydrolyze the second and third ethyl groups in basic solutions.[47−49] The heating dynamics for the autoclave used in this study were also examined. Heating from room temperature to 180 °C was observed to take 4 h (Figure 3). Thus, the use of TEP necessitates a two-step film deposition process. The first step, which occurs between 0 and 4 h, encompasses the heating of the reaction mixture from room

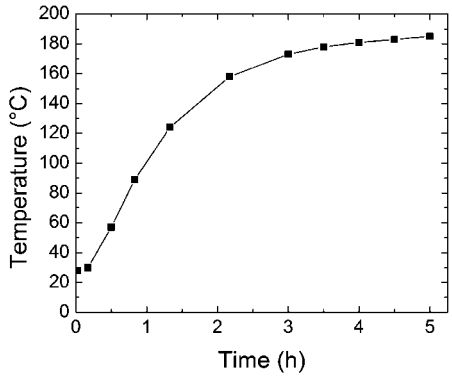

Figure 3. Autoclave heating dynamics were investigated by direct placement of K-type thermocouples into autoclaves placed in an oven preheated to 200 °C and filled with a model nonvolatile liquid, technical grade glycerol.

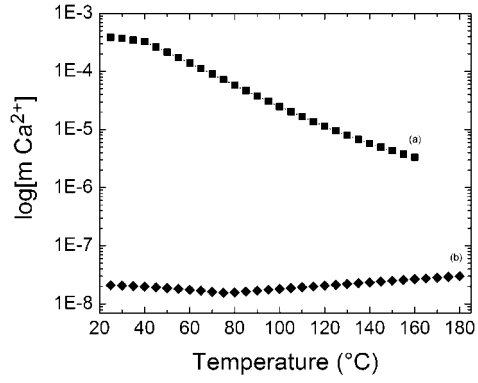

Figure 4. Thermochemical modeling of Ca^{2+} concentration (m = molal) versus temperature as a function of ionic calcium species in a hydrothermal reaction solution containing (a) 0.05 molal $CaCl_2$−0.05 molal Na_2H_2EDTA−0.05 molal NaH_2PO_4−NaOH−H_2O and (b) 0.232 molal $Ca(NO_3)_2$−1.852 molal KOH−0.232 molal EDTA−H_2O, both in the presence of titanium.

temperature to 180 °C. During this step incomplete TEP hydrolysis and the absence of free phosphate ions exclude the possibility of HA crystallization. In the second step, after 4 h, the autoclave is heated from 180 °C to the final isothermal temperature of 200 °C, complete TEP hydrolysis occurs, and free phosphate is available for the formation of HA.

(c) Equilibrium Ca^{2+} Concentration. The equilibrium concentration of uncomplexed Ca^{2+} in the 0.232 molal $Ca(NO_3)_2$−1.852 molal KOH−0.232 molal EDTA−Ti reaction mixture used in this study is displayed in Figure 4. When phosphate is first available from TEP hydrolysis at 180 °C (see above), the model calculates an uncomplexed Ca^{2+} concentration of 3.02×10^{-8} molal at a pH of 10.91. For comparison, the concentration of uncomplexed Ca^{2+} in the 0.05 molal $Ca(EDTA)^{2-}$−0.05 molal NaH_2PO_4−NaOH−H_2O−Ti hydrothermal synthesis system, demonstrated by Fujishiro et al. to form phase pure HA in this system, was modeled.[38] Thermochemical modeling of the system reported by Fujishiro et al. predicts an uncomplexed Ca^{2+} concentration of 3.31×10^{-6} molal at their initial HA deposition temperature and pH, 160 °C, pH 6. Results demonstrate that Fujishiro et al.'s system has a 2 orders of magnitude greater concentration of uncomplexed Ca^{2+} than the system reported here, at each system's respective initial HA deposition temperature. The concentration of calcium precursor used in the study reported here, however, is nearly 5-fold greater than the concentration of calcium precursor used by Fujishiro et al. The explanation for this result is pH. The literature has reported that increasing the pH of a solution decreases the ability of the Ca−$EDTA^{2-}$ complex to dissociate.[34,36] At 180 °C, the pH of the solution used in this study is thermodynamically calculated to be 10.91, at 160 °C the pH of Fujishiro et al.'s solution is 6. Thus, by using $EDTA^{4-}$, increasing pH, and having a lower concentration of uncomplexed Ca^{2+}, this synthesis process should favor crystal growth over crystal nucleation resulting in films that have a characteristic shape, and high crystallinity.[44] In addition, multiple authors have reported that the length and/or aspect ratio of HA crystals formed in solution by nonstirred homogeneous precipitation using EDTA are a function of Ca^{2+} concentration together with PO_4^{3-} concentration, EDTA/Ca ratio, temperature, and pH, indicating that a variation in grain aspect ratio should be expected from that reported elsewhere.[45,46]

(d) Substrate Characterization. Figures 5 and 6 display complementary scanning electron micrographs and X-ray diffraction patterns of Ti6Al4V, Ti, roughened Ti6Al4V, stainless steel, and Co28Cr6Mo substrates prior to hydrothermal treatment. SEM micrographs demonstrate that all nonroughened substrates lack distinct features or topography except for periodic polishing marks. The grit-blasted Ti6Al4V substrate, on the other hand, has an irregular crevassed surface with numerous pits of different sizes and shapes. These differences in surface topography are reflected in the profilometer surface roughness results reported in Table 1. Phase analysis of XRD patterns, reported in Table 1, confirm the expected identity of each material. Corundum is found in the roughened Ti substrate due to the use of Al_2O_3 media, and its implantation into the substrate during the grit-blasting process. This finding is in agreement with other authors using the same roughening technique.[17,20] Peak ratio texture analysis results are reported in Table 1 as well. Through comparison with Powder Diffraction File standards, it can be concluded that all substrates display some degree of preferred crystallographic orientation.

(e) Film Phase and Crystallinity. Figure 6 displays X-ray diffraction patterns of films deposited on Ti6Al4V, Ti, roughened Ti6Al4V, stainless steel, and Co28Cr6Mo substrates after hydrothermal treatment. Phase analysis confirms that HA is the only Ca−P phase formed on each substrate. The films formed on the Ti6Al4V, Ti, and roughened Ti6Al4V also display a small peak at 26.98° that is at the same position of the 100% TiO_2 (110) peak. All films were calculated to have crystallinity indexes of 99% because no ACP hump was identified by the analysis software for any sample (Table 2). The lack of an amorphous hump made any affect of preferred orientation, see below, on peak areas and, thus, the crystallinity calculation moot. Nonetheless, a crystallinity index less than 100% is reported because of the inherent error in the calculation. These results demonstrate that the hydrothermal crystallization process presented here deposits highly crystalline, Ca−P phase-pure HA regardless of substrate chemistry, crystallography, or surface roughness

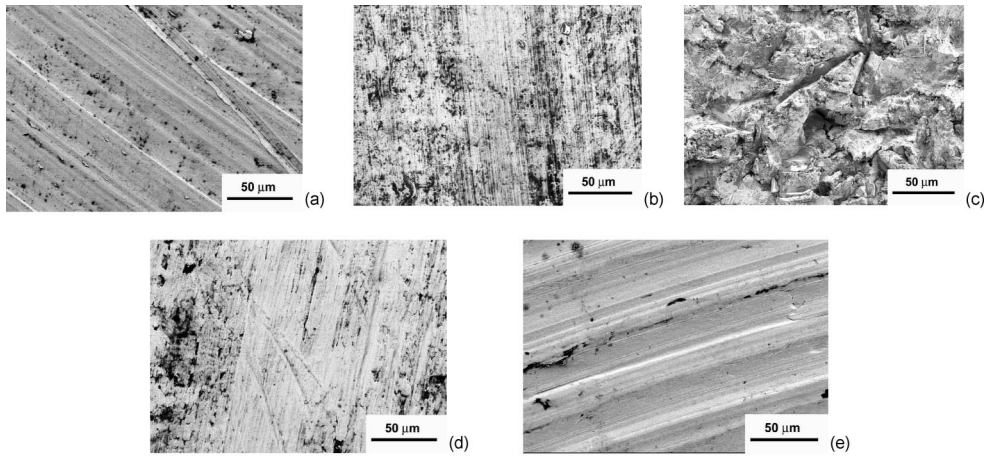

Figure 5. Scanning electron micrographs of various substrates before hydrothermal treatment: (a) Ti6Al4V, (b) Ti, (c) roughened Ti6Al4V, (d) 316 stainless steel, (e) Co28Cr6Mo alloy (magnification ×500).

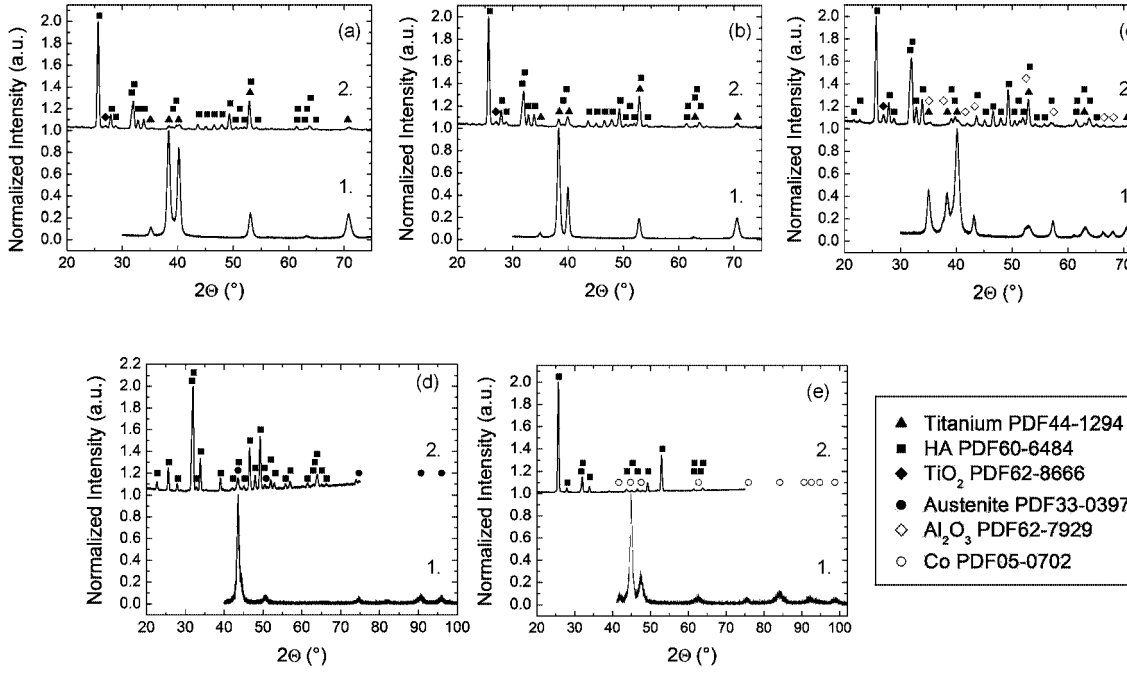

Figure 6. X-ray diffraction patterns of various substrates before and after hydrothermal treatment for 24 h at 200 °C: (a) Ti6Al4V, (b) Ti, (c) roughened Ti6Al4V, (d) stainless steel, (e) Co28Cr6Mo alloy. For each substrate: (1) prehydrothermal treatment, (2) posthydrothermal treatment.

Table 1. Substrate Roughness, Phase, and Relevant XRD Peak Ratios

substrate	roughness, Ra (nm)	identified phase(s)	Ti (0002)/ ($10\bar{1}1$)	austenite (200)/(111)	Co (0002)/ ($10\bar{1}1$)
Ti6Al4V	414	Ti	1.19		
Ti	1172	Ti	2.16		
rough-Ti6Al4V	3569	Ti, corundum	0.36		
stainless steel	531	austenite		0.05	
Co28Cr6Mo	678	Co			3.24
PDF 44−1294		Ti	0.3		
PDF 33−0397		austenite		0.45	
PDF 05−0727		Co			0.6

Table 2. Deposited Film Crystallinity, (0002)/($21\bar{3}1$) Peak Ratio, Particle Size, Thickness, and Adhesion Rating

substrate	HA crystallinity (%)	(0002)/ ($21\bar{3}1$)	avg particle diameter (μm)	thickness (μm)	adhesion rating
Ti6Al4V	99	15.26	12 ± 4	22 ± 8	5A
Ti	99	14.51	12 ± 4	13 ± 3	5A
rough-Ti6Al4V	99	4.04	11 ± 2	18 ± 4	5A
stainless steel	99	0.66	8 ± 5	16 ± 7	4A
Co28Cr6Mo	99	≫100	8 ± 5	12 ± 7	3A

(Figures 5 and 6, Tables 1 and 2). Phase-pure, high crystallinity HA is a requirement of next-generation HA films because of the lower solubility and higher bone apposition percentages that have been reported for HA coatings with increasing chemical stability.[5,16,19,52]

(f) Film Morphology and Orientation. Figure 7 displays scanning electron micrographs of films deposited on Ti6Al4V, Ti, roughened Ti6Al4V, stainless steel, and Co28Cr6Mo substrates after hydrothermal treatment. Deposited films are composed of uniform hexagonally faceted grains that appear to have grown perpendicular to the substrate surface on all substrates. The hexagonal prism is one of the idealized forms of crystals in HA's 6/m crystal class.[44] The formation of grains of this type indicates that these films form through a low energy growth controlled process.[53] This HA morphol-

(52) Fulmer, M. T.; Ison, I. C.; Hankermayer, C. R.; Constantz, B. R.; Ross, J. *Biomaterials* **2002**, *23*, 751–755.

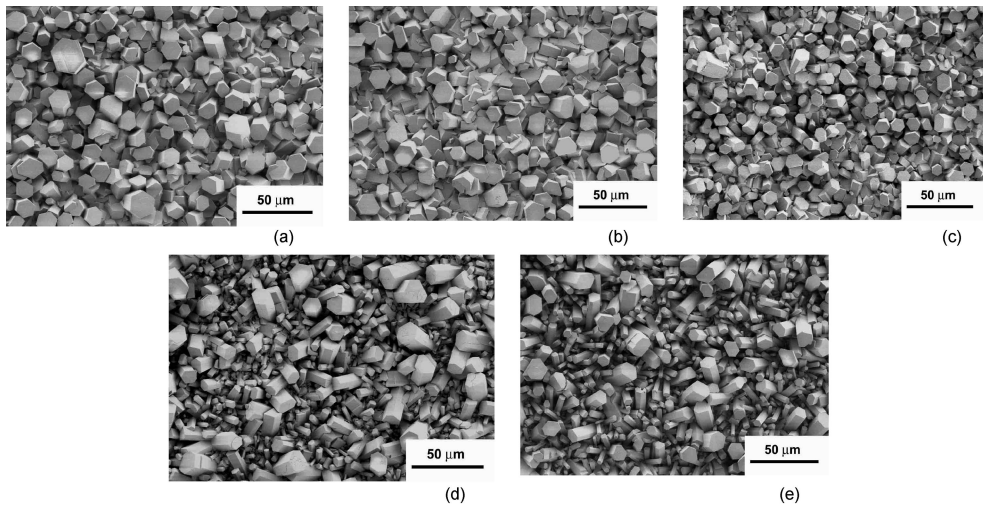

Figure 7. Scanning electron micrographs of films deposited on various substrates after hydrothermal treatment for 24 h at 200 °C: (a) Ti6Al4V, (b) Ti, (c) roughened Ti6Al4V, (d) stainless steel, (e) Co28Cr6Mo alloy (magnification ×500).

ogy is important biologically as it known to display crystallographic faces that bind bone proteins and bone protein amino acid sequences with high affinity.[41−43]

Average grain diameter and grain diameter uniformity are observed to vary from titanium-based substrates, 12 ± 4 μm, to nontitanium substrates, 8 ± 5 μm (Figure 7, Table 2). *t* test analysis of results demonstrate, however, that differences are not significant for $\alpha = 0.05$. From this result, it may be concluded that substrate chemistry and surface roughness do not play a significant role in grain nucleation and growth. Average grain diameters are larger than elsewhere in the literature, and 3−4 fold larger than those reported by Fujishiro et al., at the synthesis conditions modeled above.[36−40] Assuming that grains are continuous from the substrate surface to the film surface, a rough estimate of grain aspect ratio of 1−2 may be calculated by comparing average grain diameter to average film thickness, reported below, for each substrate. Grain aspect ratios for HA films reported elsewhere in the homogeneous precipitation hydrothermal literature are on the order of 10.[37−39,54] Thus, it may be concluded that the synthesis conditions reported here compose a novel set that enable the growth of near equiaxed hexagonal grains of HA.

X-ray diffraction peak ratio texture analysis results report (0002)/(21$\bar{3}$1) HA peak ratios that are larger than what is predicted for randomly oriented grains, 0.28, by the Powder Diffraction File, for films formed on all substrates (Figure 6, Table 2). From these results it may be concluded that hexagonal grains within all HA films are preferentially oriented with respect to the (0002) crystallographic plane regardless of substrate. Peak ratios vary from 0.66 to greater than 100 (Table 2); however, it is not appropriate to draw conclusions from these differences. Peak ratio texture analysis is a qualitative technique used to determine the presence or lack or crystallographic texture in a sample, not the degree of texture.[55] Techniques such as X-ray diffraction pole figures are required to determine the degree of texture. In a follow-up manuscript, we will report detailed time-elapsed XRD, SEM, and X-ray pole figure analysis of crystallographic orientation evolution on Ti6Al4V substrates as a function of hydrothermal reaction time.[56]

Analysis of substrate XRD patterns report that Ti6Al4V, grit-blasted Ti6Al4V, Ti, and Co28Cr6Mo substrates have (0002) crystallographic orientation and hexagonal crystal lattices (Figure 6, Table 1). Because HA also has a hexagonal crystal lattice, these results, together with the results of HA film preferred orientation analysis (Figure 6, Table 1), suggest that (0002) HA crystallographic orientation is due to epitaxy. The film formed on the nonhexagonal, non-(002) oriented 316 stainless steel, however, has a (0002)/(21$\bar{3}$1) ratio larger than the value reported in PDF 60−6484. Thus, it may be concluded that the source of grain orientation is not epitaxy, but instead a process such as competitive growth, which also results in preferentially oriented films.[57] This conclusion agrees with results from the hydrothermal literature that also report larger than predicted (0002)/(21$\bar{3}$1) HA peak ratios for films formed on nonhexagonal iron and alumina after hydrothermal treatment.[35,36]

(g) Passivation. Scanning electron micrographs are displayed in Figure 8 of cross-sections from films deposited on Ti6Al4V, Ti, roughened Ti6Al4V, stainless steel, and Co28Cr6Mo substrates after hydrothermal treatment. All micrographs display an irregular structure with grains emanating from underlying dense, continuous, passivating films. The delamination of the film formed on Co28Cr6Mo could be an artifact of the polishing process or be related to film−substrate adhesion results reported below (Figure 8e). Passive film growth models and results report that the formation of a passivating film occurs through a single process: an initial 2D film is

(53) Zwicky, F. *Rev. Mod. Phys.* **1934**, *6*, 193–208.
(54) Ha, J. S. *J. Korean Ceram. Soc.* **2003**, *40*, 1154–1158.
(55) Jones, J. L.; Slamovich, E. B.; Bowman, K. J. *J. Mater. Res.* **2004**, *19*, 3414–3422.
(56) Haders, D. J.; Burukhin, A.; Huang, Y.; Cockayne, D. J. H.; Riman, R. E. **2008**, in preparation.
(57) Thompson, C. V. *Annu. Rev. Mater. Sci.* **2000**, *30*, 159–190.

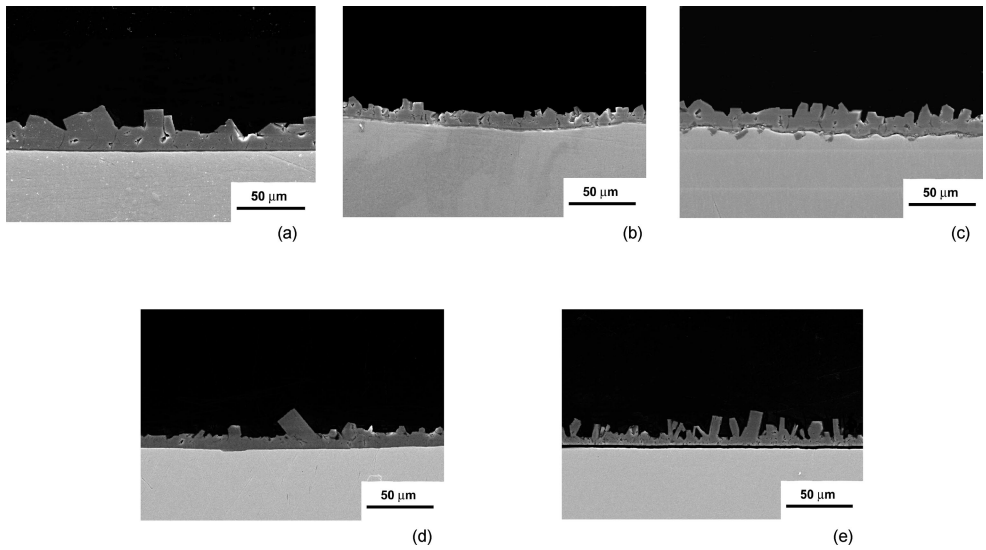

Figure 8. Scanning electron micrographs of the cross-sections of films deposited on various substrates after 24 h of hydrothermal treatment at 200 °C: (a) Ti6Al4V, (b) Ti, (c) roughened Ti6Al4V, (d) stainless steel, (e) Co28Cr6Mo alloy (magnification ×500).

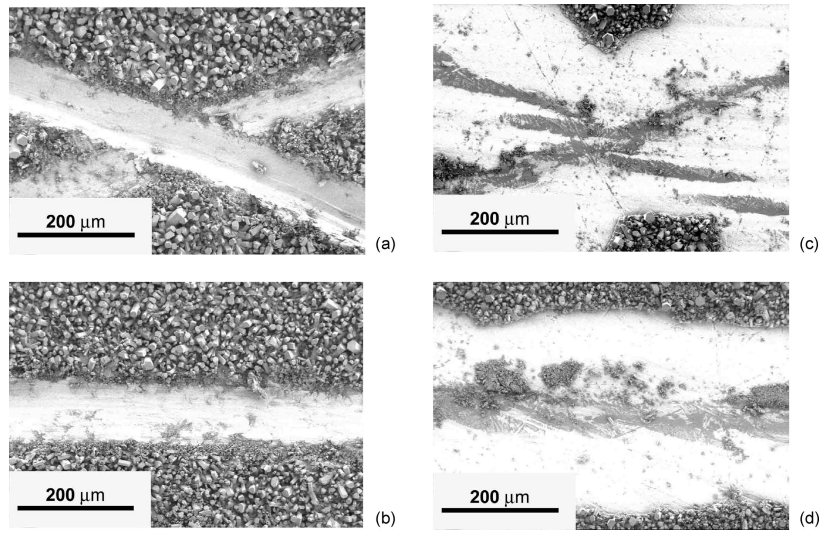

Figure 9. Scanning electron micrographs of the surface of representative hydroxyapatite films deposited on substrates by hydrothermal treatment (24 h at 200 °C) after adhesion testing: (a) roughened Ti6Al4V, (b) roughened Ti6Al4V, (c) Co28Cr6Mo alloy, (d) Co28Cr6Mo alloy.

formed followed by 3D growth.[58] Thus, the formation of passivating films on all substrates indicates that the nucleation and growth process is similar on each substrate. Average film thickness values vary from 22 ± 8 μm (Ti6Al4V) to 12 ± 7 μm (Co28Cr6Mo) (Table 2). Because of the limited area sampled by a cross-section and the topology of the samples it is not possible to draw conclusions regarding differences in film thickness from one substrate to another. Nonetheless, the formation of a dense, passivating film is important because it has the potential to inhibit the dissolution of toxic metal ions from substrates into the surrounding tissue.[24,25] The chemical stability of crystalline HA together with the passivation of the substrate surface may make this crystallization process appropriate for anticorrosion applications as well.

(h) Adhesion. Results of adhesion testing are reported in Table 2 and Figure 9. According to the standardized ASTM-D3359-02 adhesion scale of 0−5, the films deposited on Ti6Al4V, Ti, and roughened Ti6Al4V substrates scored a 5. Further, scanning electron microscopy analysis of the surface of a representative titanium substrate indicates no peeling or film removal outside the line directly cut with a razor blade. At the intersection of the cross cut, the film forms sharp points indicating strong film adhesion. The films deposited on 316 stainless steel substrates scored an average rating of 4. These films demonstrated variability in adhesion, however. Two of four samples received a rating of 4, one sample received a rating of 5, and one sample received a rating of 3. Films deposited on Co28Cr6Mo substrates scored an adhesion rating of 3. Scanning electron micrographs of the surface of a representative Co28Cr6Mo substrate display consistent and jagged film removal on either side of the original cut. Extensive film removal inhibits the formation of sharp points at the intersection of the cross cut. These results demonstrate that adhesion is a function of substrate chemistry, and primarily related to the presence of titanium

(58) Nainville, I.; Lemarchand, A.; Badiali, J.-P. *Phys. Rev. E* **1996**, *53*, 2537–2546.

in a substrate. Next generation HA films require high HA film−substrate adhesion to eliminate in vivo coating delamination and its resulting complications, which are known to increase the failure rate of PS-HA coatings.[7,11,21,22]

Discussion

The engineering of the crystallization process was facilitated by the use of thermodynamic process simulation. Through the use of process-simulation methods reported by Riman et al., phase stability diagrams were developed at 200 °C that allowed reactant concentration and pH combinations, favorable for HA deposition on multiple substrates, to be chosen prior to experimental work (Figure 2).[32,50] This eliminated the need to undertake time-consuming trial and error laboratory methodologies.

TEP hydrolysis kinetics studies revealed that under the chosen reaction conditions, free phosphate was not available for HA synthesis until 180 °C at 4 h synthesis time (Figure 4). Thus, the use of a delayed release phosphate source provided the opportunity to deposit HA-substrate intermediates prior to TEP hydrolysis, and HA posthydrolysis in a continuous crystallization process. This is in contrast to processes reported in the literature, which require multiple reaction solutions to form $CaTiO_3$−HA films on titanium substrates that improve film−substrate adhesion.[33,37,39] Results from ASTM-D3359-02 tape test A demonstrated that films formed on titanium-based substrates, regardless of alloying components or surface roughness, possessed superior adhesion properties to films formed on 316 stainless steel and Co28Cr6Mo alloy (Tables 1 and 2, Figure 9). Consequently, the explanation for this result is likely the formation of a substrate−HA chemical intermediate on titanium based substrates, $CaTiO_3$, but not on 316 stainless steel or Co28Cr6Mo prior to HA deposition. Because of the thickness of the HA film and the limited detection capabilities of X-ray diffraction, it is possible that an interfacial phase could go undetected by XRD. The film−Ti6Al4V substrate interface is examined in detail in a follow-up manuscript by Haders et al.[56]

Thermodynamic process simulation facilitated the choice of reaction conditions that both were in the region of HA phase stability and regulated the amount of uncomplexed Ca^{2+}. Thermodynamic process simulation results reported a two orders of magnitude lower Ca^{2+} ion concentration for the hydrothermal system in this study than the hydrothermal system reported by Fujishiro et al., at their respective HA deposition temperature and pH[38] (Figure 3). On the basis of the results of other hydrothermal HA film crystallization processes, this is a result of the decreased ability of the $Ca-EDTA^{2-}$ complex to dissociate in solutions with increasing pH.[34,36] By lowering Ca^{2+} concentration, it was hypothesized that the reaction conditions used here would favor crystal growth over crystal nucleation.

Growth-dominated film crystallization processes typically result in films with grains that have a characteristic shape and high crystallinity.[44] Results reported above show that uniform morphological films composed of phase-pure, high crystallinity, hexagonal-faceted HA grains were formed on all substrates. Therefore, it may be concluded that the use of pH together with the $Ca-EDTA^{2-}$ complex regulate the HA hydrothermal crystallization process by reducing the concentration of supersaturating Ca^{2+} ions, enabling the engineering of a growth-controlled crystallization process.

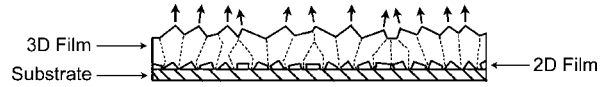

Figure 10. Proposed film growth mechanism−competitive polycrystalline film growth−as concluded from cross-sectional SEM and XRD orientation results using square facetted grains with a (111) fast growth direction to explain the process. Initially, a passive 2D film is formed. Subsequently, thickening of the initial 2D film leads to the termination of grains with (010), (100), and (001) texture by crystals with (111) texture. This occurs because the crystals with (111) texture are oriented to have their fast growth direction normal to and in the plane of the film. Adapted from Thompson et al.[57] and reprinted with permission from the *Annual Review of Materials Science* (Copyright 2000, Annual Reviews, www.annualreviews.org).

Grain aspect ratio is reportedly a function of Ca^{2+} concentration along with PO_4^{3-} concentration, EDTA/Ca ratio, temperature, and pH.[45,46] Results reported above demonstrate that the HA grains formed in this study have the largest diameters (8−12 μm) and smallest aspect ratios (1−2) reported in the homogeneous precipitation hydrothermal HA film literature. A comparison of results from the literature cited above demonstrates an interdependence of the crystallization variables noted above, which makes it difficult to definitively conclude why a nearly equiaxed aspect ratio was achieved in this study. Nonetheless, these conditions may be added to the literature to aid further understanding of the relation between grain aspect ratio and synthesis conditions.

The growth mechanism of the films may be inferred from cross-sectional SEM and top-on SEM results (Figures 7 and 8). Evaluation of cross-sectional samples revealed the formation of dense, continuous, passivating films on all substrates. On the basis of passive film growth theory and data, film formation occurs through the development of an initial 2D film followed by 3D growth.[58] Evaluation of the surface and the cross-section of films indicate that after the formation of a passive 2D film, hexagonal grains grow independently and vertically, with their *c*-axis orthogonal to the substrate surface. The topology of the surface confirms this observation. This growth model follows XRD orientation results (Figure 6, Table 2), which suggest polycrystalline film thickening by competitive growth theory.[57] Figure 10 graphically illustrates this growth process. This topic is further studied further in a follow-up manuscript by Haders et al.[56]

Conclusions

Thermodynamic process simulation facilitates the engineering of hydrothermal processes for the development of designer hydroxyapatite films. The results presented here extend our ability to use equilibrium diagrams to explore processing variable space from HA particles to HA films. The use of a TEP/EDTA doubly regulated hydrothermal crystallization scheme, the first reported in the literature, enables both the growth controlled hydrothermal crystallization of passivating HA films on numerous substrates, and apparently, the deposition of HA−substrate intermediates that improve film adhesion in a single continuous process. These results emphasize that hydro-

thermal synthesis is particularly well suited to the crystallization of designer films with controlled size, morphology, crystallinity, phase, adhesion, and conformance for orthopedic and nonorthopedic applications.

Abbreviations

HA, hydroxyapatite; PS-HA, plasma sprayed hydroxyapatite; EDTA, ethylenediamine-tetraacetic acid, $C_{10}H_{16}N_2O_8$; TEP, triethyl phosphate, $C_6H_{15}O_4P$; Ca−P, calcium−phosphate; XRD, X-Ray diffraction; ACP, amorphous calcium phosphate; FESEM, field-emission scanning electron microscopym; PDF, powder diffraction file; ASTM, American Society for Testing and Materials; Ti6Al4V, alloyed titanium with 6 wt % aluminum and 4 wt % vanadium; Co28Cr6Mo, alloyed cobalt with 28 wt % chromium and 4 wt % molybdenum.

Acknowledgment. We gratefully acknowledge research support from the Rutgers Center for Ceramic Research, the National Science Foundation/Rutgers IGERT on Biointerfaces, the Department of Education/Rutgers GAANN in Molecular, Cellular, and Nanosystems Bioengineering, the Rutgers University Graduate School New Brunswick, the New Jersey Center for Biomaterials, and the Rutgers University Roger G. Ackerman Fellowship. The authors wish to thank Valentin Starovoytov for sputter coating film cross-sections and Stryker Orthopaedics for donating Co28Cr6Mo samples.

CM071628C